Journal of Computational Physics 488 (2023) 112193

Contents lists available at ScienceDirect

Journal of Computational Physics

journal homepage: www.elsevier.com/locate/jcp

Coupling Navier-Stokes and Gross-Pitaevskii equations for the numerical simulation of two-fluid quantum flows

Marc Brachet [a], Georges Sadaka [b], Zhentong Zhang [b], Victor Kalt [b], Ionut Danaila [b,*]

[a] ENS, Université PSL, CNRS, Sorbonne Université, Université de Paris, Laboratoire de Physique de l'École Normale Supérieure, F-75005 Paris, France
[b] Univ Rouen Normandie, CNRS, Laboratoire de Mathématiques Raphaël Salem, UMR 6085, F-76000 Rouen, France

ARTICLE INFO

Article history:
Received 14 November 2022
Received in revised form 27 April 2023
Accepted 28 April 2023
Available online 5 May 2023

Keywords:
Gross-Pitaevskii
Navier-Stokes
Superfluid helium

ABSTRACT

Numerical methods for solving the Navier-Stokes equations for classical (or normal) viscous fluids are well established. This is also the case for the Gross-Pitaevskii equation, governing quantum inviscid flows (or superfluids) in the zero temperature limit. In quantum flows, like liquid helium II at intermediate temperatures between zero and 2.17 K, a normal fluid and a superfluid coexist with independent velocity fields. The most advanced existing models for such systems use the Navier-Stokes equations for the normal fluid and a simplified description of the superfluid, based on the dynamics of quantized vortex filaments, with ad hoc reconnection rules. There was a single attempt (C. Coste, 1998 [22]) to couple Navier-Stokes and Gross-Pitaevskii equations in a global model intended to describe the compressible two-fluid liquid helium II. We present in this contribution a new numerical model to couple a Navier-Stokes incompressible fluid with a Gross-Pitaevskii superfluid. Coupling terms in the global system of equations involve new definitions of the following concepts: the regularized superfluid vorticity and velocity fields, the friction force exerted by quantized vortices to the normal fluid, the covariant gradient operator in the Gross-Pitaevskii model based on a slip velocity respecting the dynamics of vortex lines in the normal fluid. A numerical algorithm based on pseudo-spectral Fourier methods is presented for solving the coupled system of equations. Finally, we numerically test and validate the new numerical system against well-known benchmarks for the evolution in a normal fluid of different types or arrangements of quantized vortices (vortex crystal, vortex dipole and vortex rings). The new coupling model has the advantage to keep the full Gross-Pitaevskii model for the superfluid, and thus describe quantized vortex dynamics without any phenomenological approximation. This opens new possibilities to revisit and enrich existing numerical results for complex quantum fluids, such as quantum turbulent flows.

* Corresponding author.
E-mail addresses: marc.brachet@gmail.com (M. Brachet), georges.sadaka@univ-rouen.fr (G. Sadaka), zhentong.zhang@univ-rouen.fr (Z. Zhang), victor.kalt@univ-rouen.fr (V. Kalt), ionut.danaila@univ-rouen.fr (I. Danaila).

https://doi.org/10.1016/j.jcp.2023.112193
0021-9991/

1. Introduction

Realistic numerical models for quantum flows, such as liquid helium below the critical (lambda) temperature $T_\lambda = 2.17K$, have to accommodate with the celebrated two-fluid model [1,2] stating that two fluids with independent velocity fields coexist in the system: a *normal* viscous fluid and an inviscid *superfluid*. If each component is taken separately, governing equations and numerical models are universally accepted: the Navier-Stokes (NS) equations for the normal fluid (the only one present in helium if $T > T_\lambda$) and the Gross-Pitaevskii (GP) equation for the superfluid (dominant for $T < 0.3K$). For intermediate temperatures, both components are present, with different physics. In the superfluid, quantized vortices are nucleated with fixed (quantized) circulation and fixed core diameter (of the atomic size). Complex interactions between quantized vortices tangled in space can lead to Quantum Turbulence (QT). In the normal fluid, vortices or eddies can develop characteristic scales from the Kolmogorov viscous scale up to the container size and eventually generate turbulence. Note that the GP equation is known to well describe low-T co-flow QT [3–6] and can be extended to describe helium equation of state and dispersion law at zero temperature [7].

Existing numerical models for quantum two-fluid flows either focus on a single component (using NS or GP models) or simplify the physics of one component in the two-fluid setting. The Hall–Vinen–Bekharevich–Khalatnikov (HVBK) model [8–10] describes the normal fluid motion by the NS model, while the superfluid motion is simplified to an Euler-like equation. The two fluids are coupled through a friction force that takes into account the influence of quantized vortices through a coarse-grained averaged superfluid vorticity. The average is considered over an ensemble of parallel (polarized) vortex filaments to find an equivalent solid-body vorticity for a dense bundle of vortex lines. The individual dynamics of quantized vortices thus disappears in the HVBK model.

A different trade-off is made in Line Vortex Navier-Stokes (LV-NS) models. Quantized vortices are described as geometrical lines, with infinite velocity and singular vorticity at the centerline. Vortex lines are moved following the Biot-Savart law. Note that the derivation of the Biot-Savart law in the context of nonlinear Schrödinger equation, when the curvature radius of vortex lines and the inter-vortex distance are much greater than the core radius, is presented in [11]. Mutual friction is described, in a more mesoscopic way, by assessing the interaction between the normal NS fluid and the vortex line dynamics [12–14]. These phenomenological LV-NS models typically contain two ingredients. First, on the vortex lines, a *slip velocity* is added to the Biot-Savart line velocity. This slip velocity is obtained as a function of the counterflow (the difference between the normal fluid velocity on the line and the line velocity) by a standard argument based on the balance of friction and Magnus forces. Second, a spatially smoothed *friction force*, opposite to the friction force acting on the line, is added as a source term in the NS equations. These vortex line models use phenomenological algorithms to deal with vortex reconnection and vortex nucleation. While recent vortex reconnection algorithms were proved to accurately describe the physics of vortex interactions when compared to experiments or GP dynamics [15,16], vortex nucleation is simply non-existent in these models. Vortex lines are individually set in the initial condition to reproduce experimentally generated vortices [17]. This could be an important limitation when modelling flows with vortices nucleated from boundaries (rough walls) or obstacles [18].

The present contribution is a first attempt, to the best of our knowledge, to directly couple incompressible NS and GP models and thus numerically simulate, without any simplification, the dynamics of a two-fluid quantum flow. The model is inspired by existing LV-NS models from which we extract the main physical ingredients of the mutual friction produced by the interaction of the normal fluid and superfluid vortices. The novelty is that we transpose this mutual friction coupling into the framework of the GP model that has the advantage to describe vortex nucleation and vortex interactions without any phenomenological assumptions [19,20]. We develop consistent expressions for the coupling with new interaction terms and we prove numerically that they are compatible with known phenomenological mutual friction laws. We first derive a *regularized line velocity field* that is smooth and reduces to the value of the line velocity, when evaluated on the vortex line. Using this regularized velocity field we build a slip velocity field that is used to couple GP and NS equations. As a main consequence of this study, coupling of NS and GP numerical codes becomes possible with this new GP-NS model.

We should mention that, in the different context of Landau's original *compressible* two-fluid model [21] describing second sound and containing neither vortices nor mutual friction, Coste [22] studied ways to couple NS and GP equations. Nevertheless, an outcome of Coste's model was to introduce a simple coupling law of the local counterflow vector to the GP equation. In the following we will use a coupling that is closely related, but different, to the one pioneered by Coste.

The paper is organized as follows. The theoretical background is given in Section 2. After first defining the uncoupled GPE and NSE equations in Section 2.1 the coupling terms are derived in Section 2.2. The numerical implementation is described in Section 2.3. Our results are contained in Section 3 and, finally, Section 4 is our conclusion.

2. Theoretical background

2.1. The uncoupled GP and NS equations

The GP equation is a partial differential equation describing the dynamics of a dilute superfluid Bose-Einstein condensate at zero-temperature. It applies to a complex field ψ, where $|\psi|^2$ is the number of particles per unit volume, and reads

$$i\hbar\frac{\partial\psi}{\partial t} = -\frac{\hbar^2}{2m}\nabla^2\psi + g|\psi|^2\psi, \tag{1}$$

where m is the mass of the condensed particles, $\hbar$ the reduced Planck constant, and g the interaction constant with $g = 4\pi\tilde{a}\hbar^2/m$ and $\tilde{a}$ the s-wave scattering length.

Equation (1) can be mapped into hydrodynamic equations for a compressible fluid by the Madelung transformation

$$\psi(\mathbf{x},t) = \sqrt{\frac{\rho(\mathbf{x},t)}{m}}\exp\left(i\frac{m}{\hbar}\phi(\mathbf{x},t)\right), \tag{2}$$

where $\rho(\mathbf{x},t)$ is the mass density of the fluid, $\phi(\mathbf{x},t)$ the velocity potential associated to the fluid velocity $\mathbf{v} = \frac{\hbar}{m}\nabla\phi$. This transformation is singular on the zeros of ψ. As two conditions are required (both real and imaginary parts of ψ must vanish), these singularities generically take the form of points in 2D and lines in 3D. The Onsager-Feynman quantum of velocity circulation around vortex lines with $\psi = 0$ is $\Gamma = h/m$. Thus, due to the multivalued nature of the velocity potential in the presence of vortex lines, the superflow is not irrotational. It can be proved [5], using the Madelung transformation, that the vorticity $\omega = \nabla\times\mathbf{v}$ is given by

$$\omega(\mathbf{r}) = \frac{h}{m}\int ds\frac{d\mathbf{r}_0}{ds}\delta(\mathbf{r}-\mathbf{r}_0(s)), \tag{3}$$

where $\mathbf{r}_0(s)$ denotes the position of the vortex line, δ is the Dirac delta function and s the arclength. Thus, the vorticity in a quantum flow is a distribution concentrated along the $\psi = 0$ topological line defects where $\mathbf{v}$ is ill-behaved (with a $1/r$ divergence).

Linearizing the GP equation around a constant state $\psi = \Psi_0$ yields the Bogoliubov dispersion relation for density plane waves ($\rho_0 e^{i(\mathbf{k}\cdot\mathbf{x}-\omega t)}$, with $\mathbf{k}$ the wave number vector):

$$\omega_B(k) = \sqrt{\frac{g\mathbf{k}^2|\Psi_0|^2}{m} + \frac{\hbar^2\mathbf{k}^4}{4m^2}}. \tag{4}$$

The sound velocity is thus given by

$$c = \sqrt{g|\Psi_0|^2/m}. \tag{5}$$

Dispersive effects take place for length scales smaller than the coherence length, defined by

$$\xi = \frac{\hbar}{\sqrt{2gm|\Psi_0|^2}}. \tag{6}$$

Note that ξ is proportional to the radius of the vortex core [3,4].

The GP equation conserves the total energy E, the total mass $\mathcal{M}$, and the momentum $\mathbf{P}$, which are defined in a volume V as

$$E = \int_V \left(\frac{\hbar^2}{2m}|\nabla\psi|^2 + \frac{g}{2}|\psi|^4\right)d^3x, \tag{7}$$

$$\mathcal{M} = m\int_V |\psi|^2 d^3x, \tag{8}$$

$$\mathbf{P} = \int_V \frac{i\hbar}{2}\left(\psi\nabla\overline{\psi} - \overline{\psi}\nabla\psi\right)d^3x, \tag{9}$$

where the overline denotes the complex conjugate.

To describe the dynamics of a viscous incompressible flow of velocity vector field $\mathbf{v}$ we use the Navier-Stokes equations

$$\partial_t\mathbf{v} + (\mathbf{v}\cdot\nabla)\mathbf{v} = -\frac{1}{\rho}\nabla p + \nu\nabla^2\mathbf{v}, \tag{10}$$

$$\nabla\cdot\mathbf{v} = 0, \tag{11}$$

where ρ is the constant flow density, ν the kinematic viscosity and p denotes the pressure field that enforces incompressibility (*i.e.* zero divergence velocity field).

The NS equations (10)-(11) conserve the total mass and the total momentum and, only for inviscid flows (with $\nu = 0$) the energy is also conserved:

$$E = \rho \int_V \frac{\mathbf{v}^2}{2} d^3x, \tag{12}$$

$$\mathcal{M} = \rho \int_V d^3x, \tag{13}$$

$$\mathbf{P} = \rho \int_V \mathbf{v} d^3x. \tag{14}$$

2.2. Building up the model

Our reasoning of model building is the following. In a nutshell, standard phenomenological Line Vortex Navier Stokes (LV-NS) models, such as those developed in [12–14], are based on the argument of cancellation of the sum of mutual friction force and Magnus force acting on the vortex line. The former is caused by the difference between the normal fluid velocity and vortex line velocity, while the latter is caused by the slip velocity, *i.e.* the difference between the vortex line velocity and superfluid velocity. This cancellation yields a phenomenological expression for the slip velocity of the vortex line that is added to the Biot-Savart expression for the equation of motion of the lines. The volume friction force that is added as a source term in the NS equation is then obtained by spatially smoothing the friction on the vortex line.

To apply the same logic to a Gross-Pitaevskii-Navier-Stokes (GP-NS) model, three separate ingredients are needed. The first one is the equivalent of the Biot-Savart velocity of vortex lines: we need a (smooth) field $\mathbf{v}_s^{reg}$ (obtained from the GP wave function ψ) that, when evaluated on vortex lines, will give the line velocities induced by the GP dynamics (in the absence of friction). Second, we need to generalize (using a volume force version) the expression of mutual friction and Magnus force cancellation. This computation will yield two results: (i) a line slip velocity field $\mathbf{v}_{\rm slip}$ which reduces on the vortex line to the standard expression used in LV-NS models and (ii) a friction force field $\mathbf{F}_{SN}$ that will be added to the right-hand side of the NS equation. Finally, as a third ingredient, we need an expression for the coupling term in the GP equation that will produce the correct slip velocity $\mathbf{v}_{\rm slip}$ of vortex lines. This coupling term is closely related, but different, to the one pioneered in [22].

2.2.1. The regularized superfluid velocity field

The superfluid velocity $\mathbf{v}_s$ can be simply defined by using the superfluid density $\rho_s = |\psi|^2$ and the relation $\mathbf{P} = \rho_s \mathbf{v}_s$ for the superfluid momentum, with $\mathbf{P}$ defined in Eq. (9). However, with line vortices present in the GP model, the associated $\mathbf{v}_s$ can also be estimated by using the Biot-Savart expression stemming from Eq. (3). Since $\mathbf{v}_s$ has singularities on the vortex line, we have to introduce a regularized velocity $\mathbf{v}_s^{reg}$ that is finite on vortex lines and yields the correct velocity circulation at large distances from vortex lines. To wit, we use the following Gaussian smoothing of the physical space field

$$\mathbf{v}_s^{\epsilon}(\mathbf{r}) = \frac{i\hbar}{2m} \frac{\psi \nabla \overline{\psi} - \overline{\psi} \nabla \psi}{\overline{\psi}\psi + \epsilon^2 \overline{\rho}_s},$$
$$\mathbf{v}_s^{reg} = (1+\epsilon^2)\, \mathcal{F}^{-1}\left(e^{-\frac{k^2}{k_{\rm reg}^2}} \mathcal{F}(\mathbf{v}_s^{\epsilon}) \right), \tag{15}$$

where $\mathcal{F}$ denotes the Fourier transform and $\overline{\rho}_s = <|\psi|^2>$ is the spatially averaged superfluid density. The smoothing wavenumber parameter $k_{\rm reg}$ is analogous to the smoothing distance used as a parameter in LV-NS models to obtain the volume force added to NS equations. Parameter ϵ is used to avoid velocity divergence on the vortex line (where $\overline{\psi}\psi = 0$) and has to be large enough to correctly resolve vortex lines. In practice (see Section 2.3), we set $\epsilon^2 = 0.1$ and $k_{\rm reg} = 1/\xi$.

The regularized velocity field allows one to define a smoothed vorticity, as the curl of the regularized velocity:

$$\mathbf{\Omega} = \nabla \times \mathbf{v}_s^{reg}. \tag{16}$$

For a straight vortex line, the effect of this Gaussian smoothing on the maximum value of smoothed vorticity, can be estimated to be F^{-1}, given by the integral

$$F^{-1} = \frac{\hbar}{2m} \frac{1}{\pi} \left[\int_{-\infty}^{\infty} e^{-\frac{k^2}{k_{\rm reg}^2}} dk \right]^2 = \frac{\hbar}{2m} k_{\rm reg}^2. \tag{17}$$

We finally define the 'normalized' vorticity field

$$\hat{\mathbf{\Omega}} = F\mathbf{\Omega} = F \nabla \times \mathbf{v}_s^{reg}, \tag{18}$$

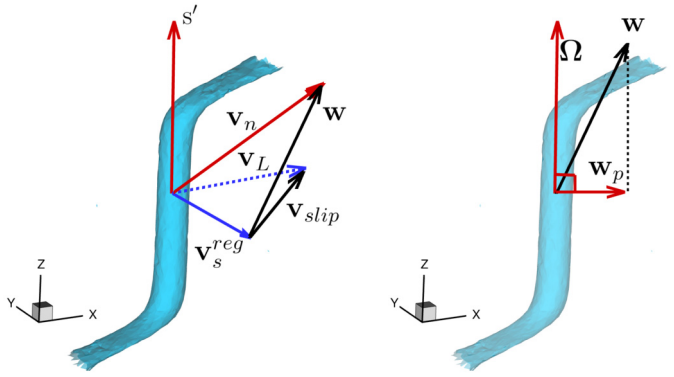

Fig. 1. Sketch of velocities acting on a vortex line.

which has a norm that is maximum and close to 1 on the vortex line and much smaller than 1 away from the vortex line.

It is important to emphasize that the role of the regularized superfluid velocity $\mathbf{v}_s^{reg}$ is only to be used as a local approximation of vortex line velocities, that will be needed to build up the coupling terms acting on NS and GP equations. In other terms, the regularized superfluid velocity is only a derived quantity from the complex GP wave function ψ. Therefore, the approximation introduced in $\mathbf{v}_s^{reg}$ does not affect the GP dynamics of the flow in the limit of very low temperatures, when no normal fluid is present.

2.2.2. Determination of the slip velocity field and volume friction force

The Magnus force density caused by $\mathbf{v}_{\rm slip}$ can be estimated starting from the momentum conservation equation [23]:

$$\mathbf{F}_{MD} = \rho_s\, \mathbf{v}_{\rm slip} \times (\nabla \times \mathbf{v}_s^{reg}). \tag{19}$$

This force density must be opposite to the force density acting on the NS fluid, thus

$$\mathbf{F}_{MD} = -\mathbf{F}_{SN}. \tag{20}$$

For $\mathbf{F}_{SN}$ we start from the simple phenomenological expression considering a force with longitudinal and transversal components

$$\mathbf{F}_{SN} \sim \rho_n \left[\beta s' \times (s' \times (\mathbf{v}_n - \mathbf{v}_L)) + \beta' s' \times (\mathbf{v}_n - \mathbf{v}_L)\right], \tag{21}$$

where ρ_n and $\mathbf{v}_n$ are the density and velocity of the normal fluid, $\mathbf{v}_L$ the velocity of the vortex line, s' the unit tangent to the line (see Fig. 1), and β, β' two phenomenological coefficients.

Using the fact that *on vortex lines* the vector $\hat{\mathbf{\Omega}} = F\mathbf{\Omega}$ is of norm 1 and directed along the line, we postulate the following formula for the volume force, equivalent to Eq. (21):

$$\mathbf{F}_{SN} = \rho_n \left[B_\star(\nabla \times \mathbf{v}_s^{reg}) \times (F(\nabla \times \mathbf{v}_s^{reg}) \times (\mathbf{v}_n - \mathbf{v}_L)) + B'_\star(\nabla \times \mathbf{v}_s^{reg}) \times (\mathbf{v}_n - \mathbf{v}_L)\right], \tag{22}$$

with $B_\star$ and $B'_\star$ the new phenomenological constants. After replacing in (20) the expressions (19) and (22), we need to solve

$$0 = -\rho_s(\nabla \times \mathbf{v}_s^{reg}) \times \mathbf{v}_{\rm slip} + \rho_n \left[B_\star(\nabla \times \mathbf{v}_s^{reg}) \times (F(\nabla \times \mathbf{v}_s^{reg}) \times (\mathbf{v}_n - \mathbf{v}_L)) + B'_\star(\nabla \times \mathbf{v}_s^{reg}) \times (\mathbf{v}_n - \mathbf{v}_L)\right]. \tag{23}$$

Because of the coupling induced slip velocity, the line velocity $\mathbf{v}_L$ is given by (see Fig. 1)

$$\mathbf{v}_L = \mathbf{v}_s^{reg} + \mathbf{v}_{\rm slip}. \tag{24}$$

Therefore (23) becomes

$$\begin{aligned} 0 = &-\rho_s\, (\nabla \times \mathbf{v}_s^{reg}) \times \mathbf{v}_{\rm slip} \\ &+\rho_n \left[B_\star(\nabla \times \mathbf{v}_s^{reg}) \times (F(\nabla \times \mathbf{v}_s^{reg}) \times (\mathbf{v}_n - \mathbf{v}_s^{reg} - \mathbf{v}_{\rm slip})) + B'_\star(\nabla \times \mathbf{v}_s^{reg}) \times (\mathbf{v}_n - \mathbf{v}_s^{reg} - \mathbf{v}_{\rm slip})\right]. \end{aligned} \tag{25}$$

A general remark on the equation to solve for $\mathbf{v}_{\rm slip}$ is that it involves two vectors fields that are obtained from the normal and superfluid components: the counterflow (see Fig. 1)

$$\mathbf{w} = \mathbf{v}_n - \mathbf{v}_s^{reg}, \tag{26}$$

and the (regularized) superfluid vorticity $\mathbf{\Omega}$ defined in (16). Recall that $\mathbf{\Omega}$ is aligned, on vortex lines, to the vector s' tangent to the line. Supposing that $\mathbf{w}$ is not aligned with $\mathbf{\Omega}$, we define the component of $\mathbf{w}$ perpendicular to the vortex line (see Fig. 1)

$$\mathbf{w}_p = \begin{cases} \mathbf{w} - \dfrac{\mathbf{w}\cdot\hat{\mathbf{\Omega}}}{|\hat{\mathbf{\Omega}}|^2}\hat{\mathbf{\Omega}}, & \text{if} \quad |\hat{\mathbf{\Omega}}| > 0, \\ \mathbf{w}, & \text{if} \quad |\hat{\mathbf{\Omega}}| = 0. \end{cases} \tag{27}$$

Note that for 2D configurations, since $\hat{\mathbf{\Omega}}$ is perpendicular to $\mathbf{w}$, Eq. (27) naturally simplifies to $\mathbf{w}_p = \mathbf{w}$ for all regions of the flow. We infer from (27) that a natural vector basis is $(\mathbf{\Omega}, \mathbf{w}_p, \mathbf{\Omega}\times\mathbf{w})$.

Using these variables, Eq. (25) becomes

$$0 = -\rho_s\, \mathbf{\Omega}\times\mathbf{v}_{\rm slip} + \rho_n\left[B_\star\mathbf{\Omega}\times(F\mathbf{\Omega}\times(\mathbf{w}-\mathbf{v}_{\rm slip})) + B'_\star\mathbf{\Omega}\times(\mathbf{w}-\mathbf{v}_{\rm slip})\right], \tag{28}$$

which is the same as

$$0 = -\rho_s\, \mathbf{\Omega}\times\mathbf{v}_{\rm slip} + \rho_n\left[B_\star\mathbf{\Omega}\times(F\mathbf{\Omega}\times(\mathbf{w}_p-\mathbf{v}_{\rm slip})) + B'_\star\mathbf{\Omega}\times(\mathbf{w}_p-\mathbf{v}_{\rm slip})\right]. \tag{29}$$

After some elementary algebraic manipulations (see details in Appendix A), we obtain closed expressions for the mutual friction, the Magnus force and the slip velocity $\mathbf{v}_{\rm slip}$. The latter is presented in the following convenient form

$$\mathbf{v}_{\rm slip} = U_\star\mathbf{w}_p + V_\star\hat{\mathbf{\Omega}}\times\mathbf{w}, \tag{30}$$

with $\hat{\mathbf{\Omega}}$ defined in (18) and

$$U_\star = \frac{\rho_n\left(B_\star^2|\hat{\mathbf{\Omega}}|^2\rho_n + B'_\star\left(\rho_s+\rho_n B'_\star\right)\right)}{B_\star^2|\hat{\mathbf{\Omega}}|^2\rho_n^2 + \left(\rho_s+\rho_n B'_\star\right)^2}, \tag{31}$$

$$V_\star = \frac{B_\star\rho_n\rho_s}{B_\star^2|\hat{\mathbf{\Omega}}|^2\rho_n^2 + \left(\rho_s+\rho_n B'_\star\right)^2}. \tag{32}$$

Note that the dimensions of the fields in the above expressions are (with L, T and M denoting units of length, time and mass): $[\mathbf{v}_{\rm slip}] = LT^{-1}$; $[\mathbf{\Omega}] = [\nabla\times\mathbf{v}_s^{reg}] = T^{-1}$; $[F] = T$, thus $[\hat{\mathbf{\Omega}}] = 1$ and $[\rho] = ML^{-3}$. In Eq. (19), $\mathbf{F}_{MD}$ is a force per volume: $[\mathbf{F}_{MD}] = ML^{-2}T^{-2}$. The same dimension is obtained in Eq. (22) for $\mathbf{F}_{SN}$ because of (20): $[\mathbf{F}_{SN}] = ML^{-2}T^{-2}$. By inspection, we conclude that the following coefficients are dimensionless: $B_\star$, $B'_\star$, $U_\star$, $V_\star$.

To summarize our results, $\mathbf{v}_{\rm slip}$ is obtained from (30)-(31)-(32) and the final expression of the friction force results from (20), (19) and (22) as

$$\mathbf{F}_{SN} = \rho_s\,\mathbf{\Omega}\times(U_\star\mathbf{w}_p + V_\star\hat{\mathbf{\Omega}}\times\mathbf{w}) = \rho_s\,\mathbf{\Omega}\times(U_\star\mathbf{w} + V_\star\hat{\mathbf{\Omega}}\times\mathbf{w}), \tag{33}$$

where we used that $\mathbf{\Omega}\times\mathbf{w}_p = \mathbf{\Omega}\times\mathbf{w}$, a relation that can be easily inferred from (27).

2.2.3. Definition of coupling terms in the GP equation

Expression (33) gives the smooth friction force field to be added to the right-hand side of the NS momentum equation (10). It is apparent by inspection that the $U_\star$ term corresponds to a force normal to the counterflow $\mathbf{w}$ and to a slip velocity parallel to $\mathbf{w}$, while the $V_\star$ term corresponds to a force parallel to $\mathbf{w}$ and a slip velocity perpendicular to $\mathbf{w}$. Therefore, on physical grounds, we expect the $V_\star$ term to remove energy from the GP dynamics (and transfer it to the NS flow) while the $U_\star$ term is expected just to change the longitudinal speed of a vortex. This point will be important in our definition of the GP coupling term.

We still need to find a way to implement the slip velocity (30) into the GP equation (1) in a way that will make the vortex lines move with an additional velocity $\mathbf{v}_{\rm slip}$. For this purpose, we consider the vortex solution of the stationary GP equation [3]. In 2D polar coordinates $(x = r\cos(\theta), y = r\sin(\theta))$ this solution representing a positive or negative vortex placed at the origin is

$$\psi_v = R(r)e^{\pm i\theta}, \tag{34}$$

and satisfies

$$0 = -\frac{\hbar^2}{2m}\nabla^2\psi_v + g|\psi_v|^2\psi_v. \tag{35}$$

The time-evolution of this vortex advected by a constant vector field $\mathbf{U}^{adv}$ is described by the partial differential equation

$$\partial_t\psi + \mathbf{U}^{adv}\cdot\nabla\psi = i\left(\frac{\hbar}{2m}\nabla^2\psi - \frac{g}{\hbar}|\psi|^2\psi\right), \tag{36}$$

with solution

$$\psi(\mathbf{r},t)=\psi_v(\mathbf{r}-t\mathbf{U}^{adv}). \tag{37}$$

Consider now the advection velocity

$$\mathbf{U}^{adv}_{\perp}=\pm\hat{\mathbf{e}}_z\times\mathbf{U}^{adv}, \tag{38}$$

where $\hat{\mathbf{e}}_z$ denotes the unit vector in the z direction, and the imaginary-time dynamics

$$\partial_t\psi-i\mathbf{U}^{adv}_{\perp}\cdot\nabla\psi=i\left(\frac{\hbar}{2m}\nabla^2\psi-\frac{g}{\hbar}|\psi|^2\psi\right). \tag{39}$$

Setting $\mathbf{U}^{adv}=(\cos(\theta^{adv}),\sin(\theta^{adv}))$ and using space and time Taylor series expansions in both positive and negative vortex cases, the vortex position $(\delta x,\delta y)$ for short times δt is given by the solution of the equation

$$(\delta x+i\delta y-e^{i\theta^{adv}}\delta t)\frac{dR}{dr}(0)=0, \tag{40}$$

showing that the position of the vortex is indeed moving with velocity $\mathbf{U}^{adv}$.

Thus, there are two different ways to move vortex lines in the GP framework with real advection velocity $\mathbf{U}^{adv}$, by adding a term which is either real (36) or imaginary (39).

The first approach (36) corresponds to that suggested in [22] and is best suited for non-dissipative processes of the GP type. Coste [22] coupled a vector $\mathbf{v}$ field to GP dynamics (1) through the following substitutions

$$\nabla\to\nabla+\frac{i}{2\alpha}\mathbf{v}, \tag{41}$$

where the short-hand notation $\alpha=\frac{\hbar}{2m}$ was used. The new gradient is similar to the covariant gradient $\nabla+i\mathbf{A}$ used in magnetic Ginzburg-Landau models, with $\mathbf{A}$ the electro-magnetic potential vector field [24]. We notice that

$$\alpha\nabla^2\to\alpha\nabla^2+i\mathbf{v}\cdot\nabla+\frac{i}{2}(\nabla\cdot\mathbf{v})-\frac{\mathbf{v}^2}{4\alpha}, \tag{42}$$

where the divergence term in the right-hand side of (42) enforces mass conservation in the modified GP equation, which becomes

$$-i\partial_t\psi=\alpha\nabla^2\psi+i\mathbf{v}\cdot\nabla\psi+\frac{i}{2}(\nabla\cdot\mathbf{v})\psi-\frac{\mathbf{v}^2}{4\alpha}\psi-\frac{g}{\hbar}|\psi|^2. \tag{43}$$

Note that, for constant $\mathbf{v}$, this is a simple Galilean boost with speed $\mathbf{v}$. Indeed, recall that the Galilean invariance of the GP equation explicitly reads:

$$\psi(\mathbf{x},t)\to\psi(\mathbf{x}-\mathbf{U}^{adv}t,t)\exp\left(i\left(\frac{\mathbf{U}^{adv}}{2\alpha}\cdot\mathbf{x}-\frac{(\mathbf{U}^{adv})^2}{4\alpha}t\right)\right), \tag{44}$$

where $\mathbf{U}^{adv}$ is the constant velocity of the boost. This transformation maps any solution $\psi(\mathbf{x},t)$ of the GP equation into another solution with associated velocity and density fields that are Galilean transforms of those associated to ψ. Thus, with $\psi_v(\mathbf{x})$ denoting as before a time-stationary vortex line solution of the GP equation, the initial data $\psi_v(\mathbf{x})\exp(i\frac{\mathbf{U}^{adv}}{2\alpha}\cdot\mathbf{x})$ corresponds to a vortex translating with (uniform) velocity $\mathbf{U}^{adv}$.

The second approach (39) is new and related to the damped Schrödinger/Gross-Pitaevskii equation [25], introducing a dissipative dynamics of the Ginzburg-Landau type. In [3], an initial data for the GP equation consisting of an array of vortex lines moving at short times with given large-scale velocity field $\mathbf{U}^{adv}$ was prepared by finding a stationary solution of the Advective Real Ginzburg-Landau Equation (ARGLE):

$$\partial_t\psi=\alpha\nabla^2\psi+(\overline{\rho}_s-\frac{g}{\hbar}|\psi|^2)\psi-i\mathbf{U}^{adv}\cdot\nabla\psi-\frac{(\mathbf{U}^{adv})^2}{4\alpha}\psi. \tag{45}$$

A solution to (45) corresponds to a minimum of the associated (modified) GP energy functional:

$$\mathcal{E}_{ARGLE}[\psi,\bar{\psi}]=\int\left(\alpha\left|\nabla\psi-i\frac{\mathbf{U}^{adv}}{2\alpha}\psi\right|^2+\left(\frac{g}{2}|\psi|^4-|\psi|^2\right)\right)d^3x. \tag{46}$$

We note that the advection term in the ARGLE Eq. (45) has opposite sign to the advection term in (39). This means, heuristically, that in an ARGLE-converged stationary state with vortices, the motion that would be created by all vortices is equally balanced by the ARGLE advection term.

Based on these mathematical-physical observations, we conclude that is necessary to split the slip velocity $\mathbf{v}_{slip}$, defined in Eq. (30), into $\mathbf{v}_{slip}^{\parallel} = U_\star \mathbf{w}_p$ and $\mathbf{v}_{slip}^{\perp} = V_\star \hat{\mathbf{\Omega}} \times \mathbf{w}$. For the coupling with GP equation we use the approach (36) with $\mathbf{U}^{adv} = \mathbf{v}_{slip}^{\parallel}$ and (39) with $\mathbf{U}_\perp^{adv}$ given by (38). Note that in our case $\mathbf{U}_\perp^{adv} = \pm(\pm\frac{\hat{\mathbf{\Omega}}}{|\hat{\mathbf{\Omega}}|}) \times (V_\star \hat{\mathbf{\Omega}} \times \mathbf{w}) = V_\star |\hat{\mathbf{\Omega}}| \mathbf{w}_p$.

Finally, the expression that has to be used for $\mathbf{v}$ in the modified GP equation (43) is

$$\mathbf{v}_{\rm slip}^{cpl} = (U_\star + iV_\star |\hat{\mathbf{\Omega}}|)\mathbf{w}_p. \tag{47}$$

Implemented in this way, the coupling corresponding to the perpendicular speed dissipates energy, as it should be, because of the work of the friction force.

It is interesting to comment on the behavior of the model in regions of low superfluid vorticity. Formula (27) for $\mathbf{w}_p$ avoids division by zero if $|\hat{\mathbf{\Omega}}| = 0$. However, if $|\hat{\mathbf{\Omega}}|$ takes very low values (*i.e.* we are very far from vortex lines) the formula (27) will generate noise in values of the velocity $\mathbf{w}_p$, by forcing it to be perpendicular to $\hat{\mathbf{\Omega}}$. Note that this problem does not arise for 2D flows for which we use directly that $\mathbf{w}_p = \mathbf{w}$. The friction force $\mathbf{F}_{SN}$ is also not affected by the noise in $\mathbf{w}_p$, since it finally depends (see Eq. (33)) only on the counterflow $\mathbf{w}$. Furthermore, following Eq. (47), the noise in $\mathbf{w}_p$ can generate noise in values of $\mathbf{v}_{\rm slip}^{cpl}$ in regions far from vortices. We note from (47) that in such regions $\mathbf{v}_{\rm slip}^{cpl} \approx U_\star \mathbf{w}_p$ and thus only the real part of the complex slip velocity could be affected by noise. In the limit $\hat{\mathbf{\Omega}} = 0$ we obtain from (31) that $U_\star \approx \rho_n/\rho_s B'_\star$, which is small, since $B'_\star$ takes low values. It is possible to remove the noise in values of $\mathbf{w}_p$ by using instead of Eq. (27) the following regularized formula

$$\mathbf{w}_p = \mathbf{w} - \frac{\mathbf{w}\cdot\hat{\mathbf{\Omega}}}{|\hat{\mathbf{\Omega}}|^2 + \epsilon_p}\hat{\mathbf{\Omega}}, \tag{48}$$

which could be applied in all regions of the flow (the division by zero is avoided). As expected from the analysis above, using small values for the constant ϵ_p in (48) will not affect the dynamics of the flow. All numerical tests in this paper were run with the two versions of the definition of $\mathbf{w}_p$ (either Eq. (27) or Eq. (48) with $\epsilon_p = 10^{-10}$) and no noticeable differences were observed in the (qualitative and quantitative) analysis of the obtained flows.

As a final remark, we note that for 2D configurations, Eqs. (27) and (48) are perfectly equivalent since $\mathbf{w}\cdot\hat{\mathbf{\Omega}} = 0$. We recall that the main simplification of the model in the 2D case is that $\mathbf{w}_p = \mathbf{w}$, which has to be applied for definitions of the slip velocity $\mathbf{v}_{\rm slip}$ (30) and final complex coupling slip velocity $\mathbf{v}_{\rm slip}^{cpl}$ (47).

2.3. Numerical coupling algorithm

We start by solving the modified Navier-Stokes equations written in the form:

$$\begin{aligned} \partial_t \mathbf{v}_n + (\mathbf{v}_n\cdot\nabla)\mathbf{v}_n &= -\frac{1}{\rho_n}\nabla p + \nu_n\nabla^2\mathbf{v}_n + \frac{1}{\rho_n}\mathbf{F}_{SN}, \\ \nabla\cdot\mathbf{v}_n &= 0, \end{aligned} \tag{49}$$

where

$$\mathbf{F}_{SN} = \rho_s\,(\nabla\times\mathbf{v}_s^{reg})\times(U_\star\mathbf{w}_p + V_\star\hat{\mathbf{\Omega}}\times\mathbf{w}), \tag{50}$$

with $\mathbf{w} = \mathbf{v}_n - \mathbf{v}_s^{reg}$, $\mathbf{w}_p = \mathbf{w} - \frac{\mathbf{w}\cdot\hat{\mathbf{\Omega}}}{|\hat{\mathbf{\Omega}}|^2}\hat{\mathbf{\Omega}}$ and $U_\star$ and $V_\star$ given by Eqs. (31) and (32), respectively. Fields $\mathbf{v}_s^{reg}$ and $\hat{\mathbf{\Omega}}$ given by Eq. (15) and (18), respectively, realize the coupling with the modified GP equation (43) in which $\mathbf{v} = \mathbf{v}_{\rm slip}^{cpl}$ from Eq. (47).

A last ingredient is necessary for the coupling model. Given that the normal fluid is assumed incompressible and that the hydrodynamic analogy of the GP equation gives a compressible fluid, we need to ensure the compatibility of the two flows and thus damp acoustic density waves in the GP flow. A standard model is the so-called damped Gross-Pitaevskii equation [26] using a dissipation term controlled by a small dimensionless parameter η_D. We thus use the following final modified GP equation:

$$\begin{aligned} \partial_t\psi = i\Bigg(&\alpha\nabla^2\psi - \gamma(|\psi|^2 - \overline{\rho}_s)\psi - \frac{1}{\alpha}\frac{(\mathbf{v}_{\rm slip}^{cpl})^2}{4}\psi\Bigg) \\ &- (\mathbf{v}_{\rm slip}^{cpl}\cdot\nabla)\psi - \frac{1}{2}(\nabla\cdot\mathbf{v}_{\rm slip}^{cpl})\psi \\ &+ \eta_D(\alpha\nabla^2\psi - \gamma(|\psi|^2 - \overline{\rho}_s)\psi + \mu\psi). \end{aligned} \tag{51}$$

Parameters $\alpha = \frac{\hbar}{2m}$ and $\gamma = \frac{g}{\hbar}$ are determined as usually from c (see Eq. (5)) and ξ (see Eq. (6)), with $|\Psi|_0^2 = \overline{\rho}_s$. Note that the value of α should be of order of the normal viscosity ν_n. The initial-data wave function is normalized to $|\psi|^2 = \overline{\rho}_s$. The term μ is introduced to ensure mass conservation in the modified GP equation.

The final system of coupled equations (49) and (51) is advanced in time using a fourth-order Runge-Kutta method (with implicit discretization of Laplacian operators). Fourier-spectral space discretization is used for both equations. The coupling algorithm was implemented in the framework of the modern parallel (MPI-OpenMP) numerical code called GPS (Gross-Pitaevskii Simulator) [27]. The GPS code was initially designed as a spectral parallel solver for the GP equation using various time-integration methods (Strang splitting, relaxation, Crank-Nicolson). It was recently used to simulate quantum turbulent flows [6]. The Navier-Stokes solver was added to the GPS code using standard Fourier pseudo-spectral method [28]. Only one external library, FFTW [29], was required for the computation. A mandatory test of the new solver was to check the energy conservation in the GP part of the code. In the absence of the normal fluid (setting $B_{tab} = B'_{tab} = 0$), 3D tests of the vortex ring evolution or reconnection of vortex rings (see Section 3.2) showed that the energy (7), decomposed as in [3,6,30], is conserved by the Runge-Kutta scheme.

The coupling model has several coefficients that have to be fixed accordingly to the physics or be adjusted numerically. To give the model a physical background, the friction coefficients $U_\star$ and $V_\star$ were linked to tabulated experimental friction coefficients B_{tab} and B'_{tab} used in the physical literature for helium II. Equivalence relations between friction coefficients are detailed in Appendix B. In the following, we prefer to set test cases using realistic values for B_{tab} and B'_{tab}. Normal ρ_n and superfluid ρ_s mass densities, the normal fluid viscosity ν_n are also fixed based on the physics of helium II, depending on the intermediate temperature between 0 and 2.17 K.

The model also includes a few numerical coefficients that have to be prescribed. These extra coefficients are the two smoothing parameters ϵ^2 and $k_{\rm reg}$ used in the definition of $\mathbf{v}_s^{reg}$ (15), and the dissipation coefficient η_D in (51). On dimensional grounds, ϵ^2 has to be a small number, $k_{\rm reg}$ has to be proportional to ξ^{-1} (the inverse of the healing length) and η_D to the physical friction coefficient B_{tab}. Remembering that ϵ^2 multiplies $\overline{\rho}_S$ (which value is close to 1), it is consistent to use $\epsilon^2 = C_\epsilon$, with C_ϵ a small value constant. We set the second coefficient in a similar way, $k_{\rm reg} = C_k \xi^{-1}$, with $C_k \leq 1$ (as commonly set in simulations of GP quantum turbulence). The values of constants C_ϵ and C_k will be adjusted in the next section by numerical tests reproducing the evolution of quantized vortices in a normal fluid.

3. Numerical results

We use in this section classical cases of vortex dynamics to numerically validate the model. We adopt the following methodology:

- The first preliminary test is more qualitative and intended to check that the coupling model produces the correct displacement of a stationary 2D quantized vortex array. The vortex crystal defined by [30] is formed by two positive and two negative vortices in a 2D domain $[0, 2\pi]^2$, with center coordinates $(\frac{\pi}{2}, \frac{\pi}{2})$ and $(\frac{3\pi}{2}, \frac{3\pi}{2})$ for the positive ones, and $(\frac{3\pi}{2}, \frac{\pi}{2})$ and $(\frac{\pi}{2}, \frac{3\pi}{2})$ for the negative vortices. This symmetric crystal arrangement has the property that $\mathbf{v}_s^{\rm reg} = 0$, and consequently $\mathbf{v}_L = \mathbf{v}_{\rm slip}$ (see Fig. 1). After obtaining the initial state of the crystal by solving the ARGLE equation (45) with $\mathbf{U}^{adv} = 0$, it is possible to impose a constant velocity $\mathbf{v}_n$ to the normal fluid (i.e. the Navier-Stokes equations are not solved) and monitor how the crystal is deformed. For $\mathbf{v}_n$ directed following the x-axis, testing only the real part of (47), the crystal remains stable and is translated by $\mathbf{v}_{\rm slip}$. When testing the imaginary term in (47), the crystal is deformed and a superfluid velocity $\mathbf{v}_s^{\rm reg}$ appears. The obtained short term behavior (pictures not shown) of the vortex crystal corresponds to this expected motion and thus confirms that the coupling model gives the correct displacement of quantized vortices in an imposed constant normal flow.
- The second numerical test is aimed at finely tune the parameters of the model (ϵ^2, $k_{\rm reg}$ and η_D) for a vortex configuration with non-trivial $\mathbf{v}_s^{\rm reg}$. For this purpose, we use the case of a 2D vortex dipole for which analytical solutions are available. The one- or two-way GP-NS coupling could be tested using this benchmark. This case is described in detail in Sec. 3.1.
- Once the values of the parameters are fixed, we test the complete coupling model by simulating the 3D dynamics of a superfluid vortex ring moving in a normal fluid. We then compare the results with those obtained by LV-NS coupling methods. We describe in Sec. 3.2 the case of a single vortex ring and the case of the head-on collision of two vortex rings, moving in a normal fluid.

3.1. 2D superfluid vortex dipole and determination of model coefficients

We consider a superfluid vortex dipole in a periodic domain $[0, 2\pi]^2$. The positive vortex (of circulation $\Gamma = \frac{h}{m} = 4\pi\alpha$) is initially centered at $(x_+, y_+) = (x_0, \pi + \frac{R_0}{2})$ and the negative vortex (of circulation $-\Gamma$) at $(x_-, y_-) = (x_0, \pi - \frac{R_0}{2})$. The dipole is moving along the x-axis, symmetrically to the center line $y = \pi$. Parameters x_0 and R_0 define the initial streamwise position of the dipole and its initial radius, respectively. In absence of normal fluid, the superfluid dipole translates in a periodic domain with known velocity [31]:

$$\mathbf{u}_s = u_s \mathbf{e}_x, \quad u_s \approx \frac{\Gamma}{4\pi}\left(\frac{1+\cos(d)}{\sin(d)} + \frac{d}{\pi}\right), \tag{52}$$

where $d = 2R = y^+ - y^-$ is the distance between vortices. If a constant normal fluid velocity is imposed along the streamwise direction ($\mathbf{u}_n = u_n \mathbf{e}_x$), the balance of forces acting on the dipole lead to the following analytical expressions for the horizontal $\dot{x}(t)$ and vertical $\dot{R}(t)$ velocities describing the dynamics of the dipole (see details in Appendix C):

$$\dot{x}(t) = \frac{\gamma_0^2 \rho_s \omega_s (u_n - u_s)}{(\gamma_0^2 + (\gamma_0' - \rho_s\omega_s)^2)(\rho_s\omega_s - \gamma_0')} + \frac{u_s \rho_s \omega_s - \gamma_0' u_n}{\rho_s \omega_s - \gamma_0'}, \tag{53}$$

$$\dot{R}(t) = \frac{\gamma_0 \rho_s \omega_s}{\gamma_0^2 + (\gamma_0' - \rho_s\omega_s)^2}(u_n - u_s), \tag{54}$$

where γ_0, γ_0' are two physical parameters related to the temperature and $\omega_s = (\nabla \times \mathbf{u}_s)\mathbf{e}_z$. Solution (53)-(54) is used in the following to finely tune the parameters of the coupling model.

3.1.1. One-way GP-NS coupling

We start by considering the one-way GP-NS coupling. The NS equations are not solved and we take $u_n = 0$, which gives simpler relations for the analytical solution (53)-(54). The superfluid vortex dipole is initially generated using the method suggested by [32] to impose the atomic density and the phase of the wave function. This case allows us to assess on the effect of the three parameters of the model:

- The *regularization wave-number* k_{reg} is necessary in Eq. (15) to obtain a smooth velocity $\mathbf{v}_s^{reg}$ and corresponding smooth vorticity $\boldsymbol{\Omega}$ in Eq. (16). It acts like a filter by smoothing the superfluid velocity and slightly diffusing the vorticity in the surrounding area of a vortex, which is the zone where the coupling force term is computed. The choice of the regulation length scale $1/k_{\text{reg}}$ was found to be critical to balance the accuracy and validity of the numerical simulation. If k_{reg} is too large (i.e. the vorticity around a vortex line is not smooth enough), the results could be more accurate, but the simulation might be unstable because of numerical oscillations (wiggles). On the other hand, if k_{reg} is too small, the numerical results are stable, but the accuracy is diminished. A trade-off between these two effects thus should be found. Figure 2 (a) shows that by decreasing k_{reg}, the vortices of the dipole approach to each other with an increasing rate. We fixed $k_{\text{reg}} = 1/\xi$, considering that a regularization length scale of the order the vortex core is physically reasonable.
- The *small parameter* ϵ^2 in Eq. (15) is also needed to avoid the singularity of the superfluid velocity when the vortex line passes near a mesh node (as $\overline{\psi}\psi$ is zero on the vortex line). We took $\epsilon^2 = 0.1$ to ensure that the corresponding effective regularization length 0.31ξ is smaller than the regularization length introduced by k_{reg}.
- The *dissipation* parameter η_D was introduced in the GP equation to damp sound (pressure) waves and thus ensure the compatibility of the model with the incompressible flow assumption for both normal and superfluid. This dissipation is also affecting the intensity of the coupling force, which suggests that is reasonable to assume that η_D is proportional to B_{tab}. Figure 2 (b) compares the numerical results with the analytical solution with different η_D. When setting $\eta_D = 0$, we found that the two vortices of the dipole do not approach to each other fast enough and the gap between their positions do not evolve any more after reaching the value of approximately 10ξ. When η_D is increased, vortices approach to each other in a increasing rate. The parameter η_D was finally fixed to the value $0.02B_{tab}$, for which the numerical solution fits perfectly to the analytical solution. When $B_{tab} = B'_{tab}$, the value $\eta_D = 0.01B_{tab}$ is also a good choice for the dissipation constant.

Figure 2 (c) shows that using the values $\epsilon^2 = 0.1$, $k_{\text{reg}} = 1/\xi$ and $\eta_D = 0.02B_{tab}$, the numerical results fit perfectly with the analytical solution for different coupling force coefficients B_{tab} and B'_{tab}. Figure 3 offers a final validation of the values found for the parameters of the model by depicting the time trajectories and time evolution of the radius of the dipole for typical values of coupling force coefficients $B_{tab} = 0.4$ and $B'_{tab} = 0.1$ (that will be used in the next sections).

3.1.2. Two-way GP-NS coupling

We now simulate the time evolution of the same 2D dipole, but with the full two-way GP-NS coupling. The parameters of the model are kept the same as determined from the one-way coupling. The difference between the two types of coupling is visible in Fig. 4. When considering the coupling force in the NS equations (two-way coupling), the vortices of the dipole approach to each other with a reduced rate. This was expected, since the moving vortex dipole generates, through the coupling force, a normal fluid velocity ($u_n \neq 0$) that finally counteracts the mutual friction. The configuration of the flow is illustrated in Fig. 5 presenting snapshots of the normal fluid vorticity and streamlines, together with the identification of the superfluid vortices by iso-contours of low-atomic density. We observe a *triple-vortex-pair* structure consisting of a pair of superfluid anti-vortex and two pairs of anti-vortex of normal fluid: the first one is surrounding the superfluid vortices and rotates in the same direction, and the second one is adjacent to superfluid vortices and rotates in the opposite direction. The streamlines show how the normal fluid is entrained by the motion of the superfluid vortex pair. By comparing the two snapshots, we can also observe that vortices move towards each other while translating downstream.

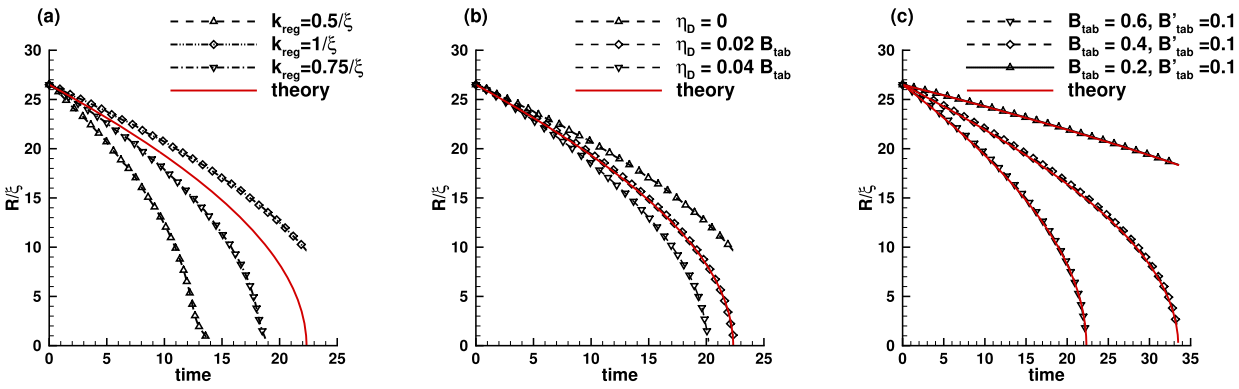

Fig. 2. 2D evolution of a superfluid vortex dipole. One-way GP-NS coupling, with $\mathbf{u}_n = 0$. Time evolution of the half distance between the two vortices normalized by the size of the vortex core ξ. Solid lines represent the analytical solution. (a) Results for three values of the smoothing wave number $k_{\rm reg}$ and common values $B_{tab} = 0.6$ and $B'_{tab} = 0.1$. (b) Results for three values of the dissipation parameter η_D and common values $B_{tab} = 0.6$ and $B_{tab} = 0.1$. (c) Results for $k_{\rm reg} = 1/\xi$, $\eta_D = 0.02 B_{tab}$, and three different choices for the coupling force parameters B_{tab} and B'_{tab}.

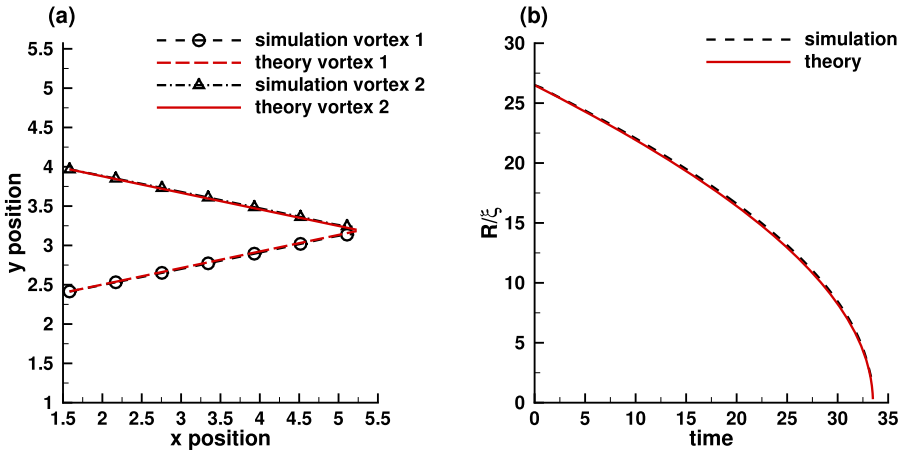

Fig. 3. 2D evolution of a superfluid vortex dipole. One-way GP-NS coupling, with $\mathbf{u}_n = 0$. Simulation with fixed parameters: B_{tab} = 0.4, $B'_{tab} = 0.1$, $d/\xi = 53$, $N = 256$, $k_{\rm reg}^{-1} = \xi$, $\eta_D = 0.02 B_{tab}$. (a) Trajectories of the two vortices. (b) Time evolution of the half distance between the two vortices normalized by the size of the vortex core.

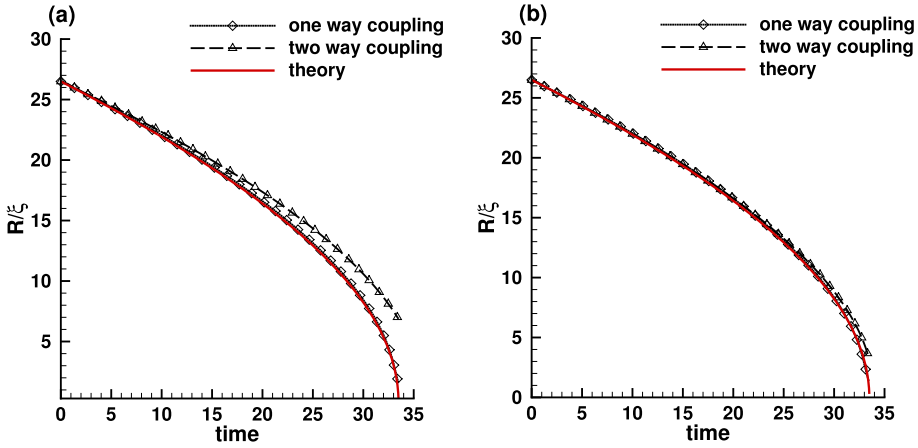

Fig. 4. 2D evolution of a superfluid vortex dipole. Time evolution of the half distance between the two vortices normalized by the size of the vortex core ξ. Comparison between $(-\diamond-)$ one-way coupling ($\mathbf{u}_n = 0$) and $(-\triangle-)$ two-way coupling ($\mathbf{u}_n \neq 0$) for different physical parameters (a): B_{tab} = 0.4, B'_{tab} = 0.1, $\eta_D = 0.02 B_{tab}$, (b): B_{tab} = 0.4, B'_{tab} = 0.4, $\eta_D = 0.01 B_{tab}$. Common parameters of the model: $d/\xi = 53$, $N = 256$, $k_{\rm reg}^{-1} = \xi$.

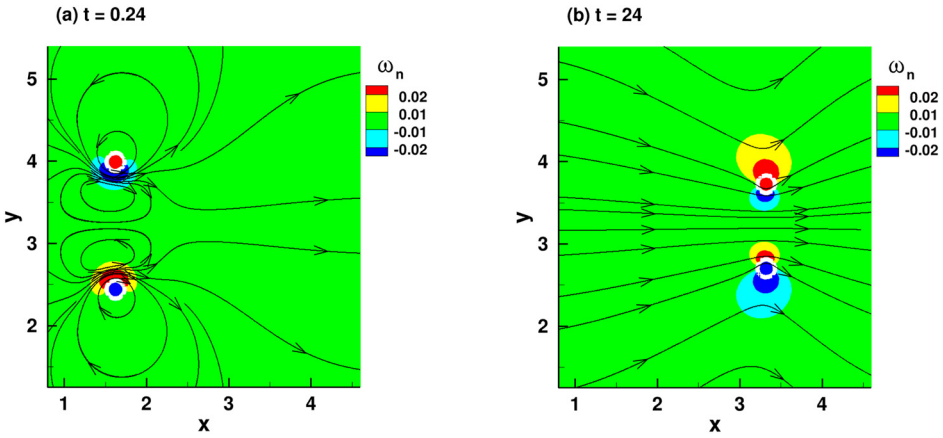

Fig. 5. 2D evolution of a superfluid vortex dipole. Two-way GP-NS coupling. Illustration of the triple-vortex structure of the flow. The entrained normal fluid is represented by its vorticity contours (colors) and streamlines (arrow black lines). Superfluid vortices (white circles) are identified by an iso-contour of low atomic density ($0.5\ |\psi|^2_{max}$). Snapshots of the flow for time instants: (a) t=0.24, (b) t=24. Parameters of the simulation: $B_{tab} = 0.4$, $B'_{tab} = 0.1$, $\eta_D = 0$, $d/\xi = 53$, $N = 256$, $k_{\rm reg}^{-1} = \xi$. (For interpretation of the colors in the figure(s), the reader is referred to the web version of this article.)

3.2. 3D superfluid vortex ring

The triple-vortex structure observed in the 2D simulation of a vortex dipole is similar to that observed in the 3D flow generated by a superfluid vortex ring moving in a normal fluid [13,14,33]. We use this case to validate in 3D our full coupling GP-NS coupling model. The initial superfluid vortex ring is generated using Padé approximations and the ARGLE procedure [6]. The normal fluid is initially at rest.

Figure 6 shows snapshots of the time evolution of the vortex ring for different physical parameters $B_{tab} = B'_{tab}$ (panels a, b) and $B_{tab} > B'_{tab}$ (panels c, d). The superfluid vortex ring (in black) moves in the x-direction from left to right and sweeps surrounding normal fluid due to the action of the coupling force. Two normal fluid vortex rings with opposite circulations are thus created, an outer one with large radius (in blue) and an inside smaller vortex ring (in red). The overall dimension of this triple-vortex rings structure reduces while moving downstream. We thoroughly investigated the influence of the values of physical parameters on the topology of the triple-vortex. When $B_{tab} \approx B'_{tab}$ the small inner normal vortex ring (in red) travels at the rear of superfluid ring, while for $B_{tab} > B'_{tab}$ it is placed slightly in front of the superfluid ring.

The triple-vortex ring structure illustrated in Fig. 6 is very similar to that recently found by LV-NS coupling models using vortex filaments for the superfluid and different NS solvers for the normal fluid [14,33]. For a more detailed comparison with LV-NS methods, we simulated the evolution of the superfluid vortex ring for temperatures ranging between 1.3 K and 2 K, as in [17]. Coefficients B_{tab} and B'_{tab} for each value of the temperature were calibrated using data from [34]. The time evolution of the radius of the vortex ring shown in Fig. 7 is similar to that reported in [17]. The vortex ring radius shrinks more rapidly if the temperature is increased, since large temperatures imply larger friction forces and dissipation. Note, however, that the scales of the flow are not the same and in our simulations the computational box is much smaller than in LV-NS methods (see the discussion in Section 4).

To emphasize the advantage of our GP-NS coupling to describe vortex interactions in superfluids without any phenomenological model, we also simulate the head-on collision of two superfluid vortex rings. In this case, superfluid vortex lines become distorted and their reconnection implies the exchange of parts of the lines and the formation of new tangled structures. This process is illustrated in Fig. 8. We use the same parameters as for the vortex ring case presented in Fig. 6 (c, d). Two vortex rings are seeded in the initial condition, with the same radius and opposite propagation directions. Vortex centers are shifted along the vertical axis, as in the recent simulation by [33], using LV-NS coupling methods. The mutual induction deforms the vortex rings when they approach to each other (Fig. 8a). The interaction (Fig. 8b) consists in the exchange of parts of each vortex line. After reconnection (Fig. 8c) the two new vortex rings are distorted and continue their movement following their original direction. This complex interaction of superfluid vortex rings trigger in the normal fluid the formation of two pairs of normal vortex rings, that are attached to the quantized vortex ring and undergo the well-known *cut-and-connect* reconnection mechanism for viscous NS vortex tubes [35,36]. The obtained image of vortex interaction is qualitatively similar to that obtained in [33] using phenomenological models for vortex reconnection, but there are differences. In particular, the repulsive motion observed when the two vortex ring are getting closer and before the connection is more intense than in LV-NS simulations. This affects the stretching of the normal fluid trapped between the two vortex rings. We recall that the superfluid vortex dynamics in our model obeys the GP equation, without any phenomenological assumption on the reconnection process.

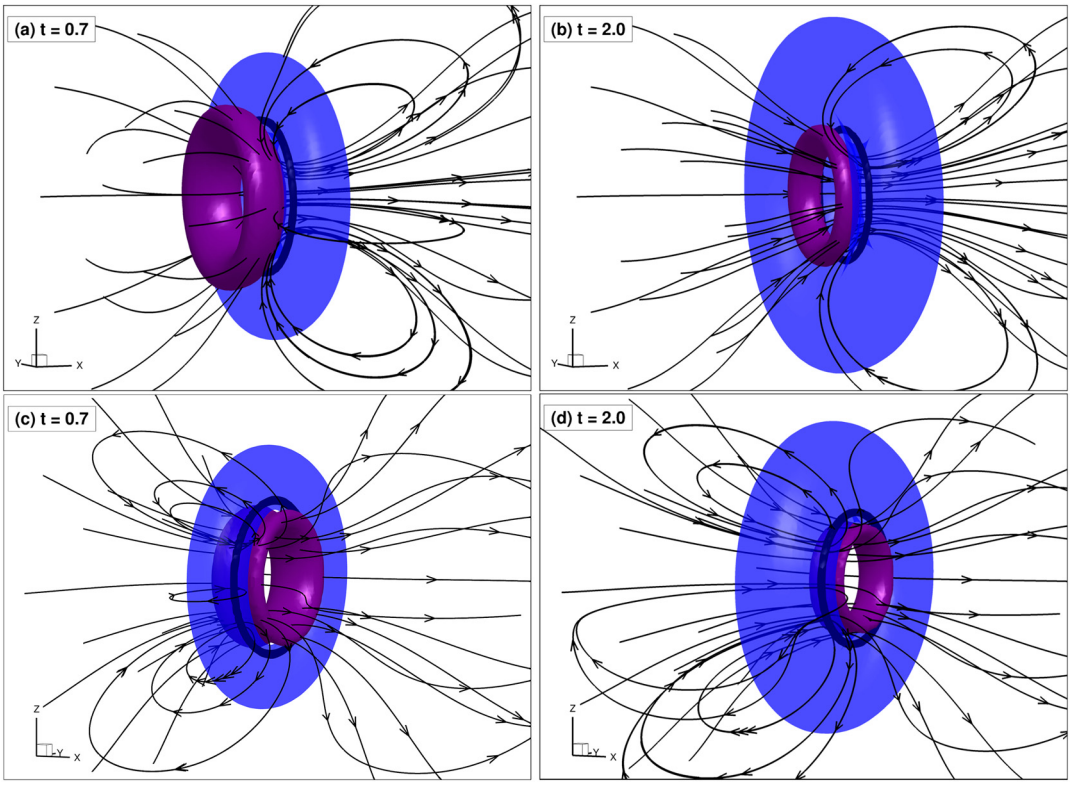

Fig. 6. 3D evolution of a superfluid vortex ring in a normal fluid initially at rest. Snapshots for two time instants. Physical parameters $\rho_n/\rho_s = 1$, $B_{tab} = B'_{tab} = 0.4$, $\eta_D = 0.035 B_{tab}$ (panels a, b), $B_{tab} = 0.4 > B'_{tab} = 0.1$, $\eta_D = 0.05 B_{tab}$ (panels c, d). Illustration of the triple-vortex structure. The superfluid vortex ring (in black) is identified by an iso-surface of low atomic density ($0.5\ |\psi|^2_{max}$). The two counter-rotating normal vortex rings are identified by iso-surfaces of normal fluid azimuthal vorticity: 0.03 for the blue outer ring and (-0.03) for the red inner ring. The streamlines in the normal fluid are also drawn. Mesh resolution 128^3.

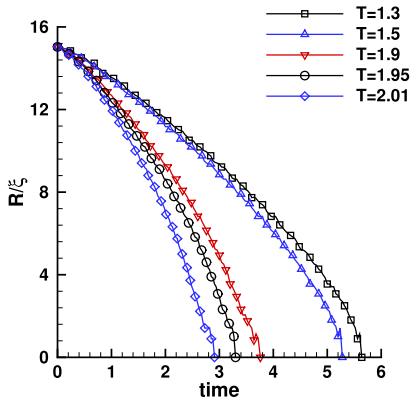

Fig. 7. 3D evolution of a superfluid vortex ring in a normal fluid initially at rest. Time evolution of the vortex ring radius for five different temperatures.

4. Conclusion

Recent models for the numerical simulation of two-fluid quantum flows (like helium II) were focused on coupling Navier-Stokes solvers for the normal fluid with vortex filaments methods for the superfluid fraction [14,33]. These models consider that the superfluid dynamics is essentially described by line-vortex interactions (Biot-Savart law) and thus referred to as LV-NS models. The resulting main drawbacks are that vortex nucleation is absent from the description and superfluid vortex reconnections are necessarily based on phenomenological assumptions. While improved vortex reconnection algorithms [15,16] can solve the second drawback, the absence of vortex nucleation prevents the direct application of LV-NS models to flows where vortices are generated by boundaries or obstacles [18]. We presented in this paper a model that links the Navier-Stokes (NS) normal flow dynamics to the Gross-Pitaevskii (GP) description of the superfluid fraction. The advantage

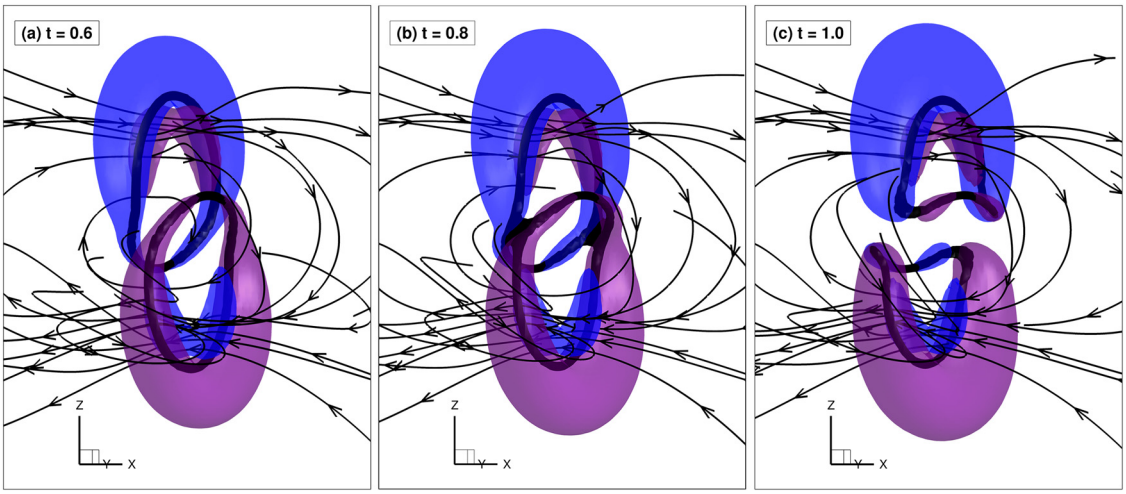

Fig. 8. 3D head-on collision of two superfluid vortex rings in a normal fluid initially at rest. Snapshots for three time instants. Physical parameters $\rho_n/\rho_s = 1$, $B_{tab} = 0.4$, $B'_{tab} = 0.1$, $\eta_D = 0.05 B_{tab}$. Illustration of the structure of vortex reconnection. The superfluid vortex ring (in black) is identified by an iso-surface of low atomic density ($0.2\ |\psi|^2_{max}$). The two counter-rotating normal vortex rings are identified by iso-surfaces of normal fluid azimuthal vorticity: 0.05 for the blue outer ring and (-0.05) for the red inner ring. The streamlines in the normal fluid are also drawn. Mesh resolution 128^3.

of the model is that superfluid vortex dynamics is accurately and naturally described by the GP equation, as universally accepted in the literature. The new GP-NS coupling model is compatible with physical concepts (mutual friction force, source term in NS) used in LV-NS models, but redefined in the framework of the GP superfluid dynamics. The modified GP equation follows some ideas introduced in [22] to describe the compressible two-fluid liquid helium II, but it introduces new concepts: the regularized superfluid vorticity and velocity fields, the covariant gradient operator in the GP equation based on a slip velocity respecting the dynamics of vortex lines in the normal fluid.

The new GP-NS coupling model was implemented in a pseudo-spectral Fourier spectral code. Intensive tests validated the new numerical system against well-known benchmarks for the dynamics of different types or arrangements of quantized vortices (vortex crystal, vortex dipole and vortex rings) evolving in a normal fluid. The simulation of superfluid vortex head-on collision proved the ability of the method to account, without any phenomenological assumption, on the complex vortex interaction and reconnection. The range of scales for which the present method is applicable is complementary to that used in VL-NS models. In our GP-NS approach, we have to resolve flow scales less than the vortex core size, which imposes an obvious computational limitation in the size of the computational box. In VL-NS models, the computational grid has to resolve the inter-vortex distance, but do not need to resolve the vortex core (vortex lines are singularities of zero thickness). Simulations with VL-NS models can therefore cover scales similar to that of experiments, while the GP-NS model offers a magnified view of the flow at the scale of the vortex core size. Our model is thus prevented to describe full scale experiments, but it offers the possibility to revisit many fundamental phenomena occurring in two-fluid quantum flows that were established using the vortex filament method for superfluids (see the recent review [26]): reconnections of superfluid vortex lines in a NS fluid, movement of superfluid vortex bundles in a normal fluid, etc.

Another fundamental question is whether the present GP-NS model could be quantitatively applied to describe two-fluid helium quantum flows. First, in order to correctly describe superfluid liquid helium, we need a correct equation of state and a dispersion relation also involving rotons excitations. This implies that the GP equation needs to be extended by including non-local and higher order nonlinear terms [37–39]. Second, the NS description itself for the normal fluid will be valid only for scales of the order, or smaller than the thermal excitation mean free path. For low temperatures the mean free path of the rotons and phonons becomes ballistic (for a detailed discussion of the involved length scales, see [14]), which indicates that NS equation should be replaced with a Boltzmann equation. A quantitative self-consistent description of the two-fluid helium flow for all range of temperatures is still an open problem. It remains to be seen if such a complete approach will provide similar results to those obtained in the present simplified GP-NS physical framework.

CRediT authorship contribution statement

Marc Brachet: Conceptualization, Methodology, Writing – original draft, Writing – review & editing. **Georges Sadaka:** Data curation, Software, Validation, Visualization. **Zhentong Zhang:** Software, Validation. **Victor Kalt:** Software, Validation. **Ionut Danaila:** Conceptualization, Funding acquisition, Methodology, Project administration, Writing – original draft, Writing – review & editing.

Declaration of competing interest

The authors declare that they have no known competing financial interests or personal relationships that could have appeared to influence the work reported in this paper.

Data availability

Data will be made available on request.

Acknowledgements

The authors acknowledge financial support from the French ANR grant ANR-18-CE46-0013 QUTE-HPC. Part of this work was performed using computing resources of CRIANN (Centre Régional Informatique et d'Applications Numériques de Normandie, France).

Appendix A. Expression of the slip velocity

To solve Eq. (29), we use that $\mathbf{v}_{\rm slip}$ is perpendicular to the vortex line: $\mathbf{v}_{\rm slip}\cdot\boldsymbol{\Omega}=0$. We obtain:

$$-\rho_s\mathbf{v}_{\rm slip}+\rho_n(B_\star(F\boldsymbol{\Omega}\times(\mathbf{w}_p-\mathbf{v}_{\rm slip}))+B'_\star(\mathbf{w}_p-\mathbf{v}_{\rm slip}))=0, \tag{A.1}$$

or

$$-(\rho_s+B'_\star\rho_n)\mathbf{v}_{\rm slip}-\rho_nB_\star F\boldsymbol{\Omega}\times\mathbf{v}_{\rm slip}=-\rho_n(B_\star F\boldsymbol{\Omega}\times\mathbf{w}+B'_\star\mathbf{w}_p). \tag{A.2}$$

Setting

$$\mathbf{v}_{\rm slip}=U_\star\mathbf{w}_p+V_\star F\boldsymbol{\Omega}\times\mathbf{w}, \tag{A.3}$$

we obtain that

$$\begin{aligned}&-(\rho_s+B'_\star\rho_n)(U_\star\mathbf{w}_p+V_\star F\boldsymbol{\Omega}\times\mathbf{w})\\&-\rho_nB_\star F\boldsymbol{\Omega}\times(U_\star\mathbf{w}_p+V_\star F\boldsymbol{\Omega}\times\mathbf{w})\\&=-\rho_n(B_\star F\boldsymbol{\Omega}\times\mathbf{w}+B'_\star\mathbf{w}_p)\end{aligned} \tag{A.4}$$

or, using that $\boldsymbol{\Omega}\times(\boldsymbol{\Omega}\times\mathbf{w})=\boldsymbol{\Omega}\times(\boldsymbol{\Omega}\times\mathbf{w}_p)=-\boldsymbol{\Omega}\cdot\boldsymbol{\Omega}\,\mathbf{w}_p$,

$$\begin{aligned}&-(\rho_s+B'_\star\rho_n)(U_\star\mathbf{w}_p+V_\star F\boldsymbol{\Omega}\times\mathbf{w})\\&-\rho_nB_\star FU_\star\boldsymbol{\Omega}\times\mathbf{w}_p+\rho_nB_\star FV_\star F\boldsymbol{\Omega}\cdot\boldsymbol{\Omega}\,\mathbf{w}_p\\&=-\rho_n(B_\star F\boldsymbol{\Omega}\times\mathbf{w}+B'_\star\mathbf{w}_p).\end{aligned} \tag{A.5}$$

Taking the inner product with $\mathbf{w}_p$ and $\boldsymbol{\Omega}\times\mathbf{w}$, we infer that

$$-(\rho_s+B'_\star\rho_n)U_\star+\rho_nB_\star V_\star F^2\boldsymbol{\Omega}\cdot\boldsymbol{\Omega}=-\rho_nB'_\star, \tag{A.6}$$

$$-\rho_nB_\star U_\star-(\rho_s+B'_\star\rho_n)V_\star=-\rho_nB_\star. \tag{A.7}$$

The final solution is

$$U_\star=\frac{\rho_n\left(B_\star^2F^2\boldsymbol{\Omega}\cdot\boldsymbol{\Omega}\rho_n+B'_\star\left(\rho_s+\rho_nB'_\star\right)\right)}{B_\star^2F^2\boldsymbol{\Omega}\cdot\boldsymbol{\Omega}\rho_n^2+\left(\rho_s+\rho_nB'_\star\right)^2}, \tag{A.8}$$

$$V_\star=\frac{+B_\star\rho_n\rho_s}{B_\star^2F^2\boldsymbol{\Omega}\cdot\boldsymbol{\Omega}\rho_n^2+\left(\rho_s+\rho_nB'_\star\right)^2}. \tag{A.9}$$

Appendix B. Expressions of friction coefficients

Friction coefficients $U_\star$ and $V_\star$ in Eq. (30) can be related to physical friction coefficients tabulated for superfluid helium II [34]. We recall that three different scales appear in our model: the healing length ξ that is also the scale of the vortex core, the smallest normal fluid length (the phonon/rotons mean free path) λ and the inter-vortex distance ℓ. In LV-NS models, since a vortex is a filament, $\xi = 0$ and $\lambda < \ell$. In HBVK models, the superfluid vorticity is averaged over a length scale larger than ℓ. In our description, we average over some intermediate scale l, supposing that $\xi < \lambda < l < \ell$, to obtain a mesoscopic description of the mutual friction.

We consider the case of a uniform rotation and use the experimentally tabulated coefficients B_{tab} and B'_{tab} given by [34]. By averaging over the vortex array, we must identify:

$$B_{tab} = \frac{\rho}{\rho_n} V_\star, \tag{B.1}$$

$$B'_{tab} = \frac{\rho}{\rho_n} U_\star. \tag{B.2}$$

The above relations for $(U_\star,\ V_\star)$ can be inverted into

$$B_\star = \frac{\rho_s V_\star}{\rho_n \left(\hat{\boldsymbol{\Omega}}^2 V_\star^2 + (U_\star - 1)^2\right)}, \tag{B.3}$$

$$B'_\star = -\frac{\rho_s \left(\hat{\boldsymbol{\Omega}}^2 V_\star^2 + (U_\star - 1) U_\star\right)}{\rho_n \left(\hat{\boldsymbol{\Omega}}^2 V_\star^2 + (U_\star - 1)^2\right)}. \tag{B.4}$$

Using the that $\hat{\boldsymbol{\Omega}}^2 = 1$ on vortex lines, we finally find for our coefficients $B_\star,\ B'_\star$:

$$B_\star = \frac{\rho_s \frac{\rho_n}{\rho} B_{tab}}{\rho_n \left((\frac{\rho_n}{\rho} B_{tab})^2 + (\frac{\rho_n}{\rho} B'_{tab} - 1)^2\right)}, \tag{B.5}$$

$$B'_\star = -\frac{\rho_s \left((\frac{\rho_n}{\rho} B_{tab})^2 + (\frac{\rho_n}{\rho} B'_{tab} - 1) \frac{\rho_n}{\rho} B'_{tab}\right)}{\rho_n \left((\frac{\rho_n}{\rho} B_{tab})^2 + (\frac{\rho_n}{\rho} B'_{tab} - 1)^2\right)}, \tag{B.6}$$

or

$$B_\star = \frac{B_{tab} \rho \rho_s}{\rho_n^2 \left({B'_{tab}}^2 + B_{tab}^2\right) - 2 B'_{tab} \rho \rho_n + \rho^2}, \tag{B.7}$$

$$B'_\star = \frac{B'_{tab} \rho \rho_s - \rho_n \rho_s \left({B'_{tab}}^2 + B_{tab}^2\right)}{\rho_n^2 \left({B'_{tab}}^2 + B_{tab}^2\right) - 2 B'_{tab} \rho \rho_n + \rho^2}. \tag{B.8}$$

Appendix C. Movement of a 2D vortex dipole in a normal fluid

We consider the superfluid vortex dipole described in Sec. 3.1. In a periodic domain and in absence of normal fluid, the superfluid dipole moves in the x-direction with the velocity given by Eq. (52) [31]. Considering that the vortices of the dipole are straight lines perpendicular to the movement plane (x, y), we can apply the force balance equation (20). We assume that the velocity induced by the vortex line is (in the vicinity of the line):

$$\mathbf{v}_s = u_s \mathbf{e}_x, \tag{C.1}$$

with u_s given by Eq. (52). Since the velocity of vortex lines is:

$$\mathbf{v}_L = \dot{x}\, \mathbf{e}_x + \dot{R}\, \mathbf{e}_y, \tag{C.2}$$

the tangent vector is $s' = \mathbf{e}_z$ and the vorticity $\boldsymbol{\Omega} = \omega_s \mathbf{e}_z$, we can use Eqs. (19), (20), and (22) to obtain:

$$0 = \rho_s \omega_s \mathbf{e}_z \times (\mathbf{v}_L - \mathbf{v}_s) + \gamma_0 (\mathbf{v}_n - \mathbf{v}_L) + \gamma'_0 \mathbf{e}_z \times (\mathbf{v}_n - \mathbf{v}_L), \tag{C.3}$$

with $\gamma_0 = \rho_n B_\star / F$ and $\gamma'_0 = -\rho_n B'_\star$. Assuming that $\mathbf{v}_n = u_n \mathbf{e}_x$, we separate from relation (C.3) the two linear equations corresponding to x and y directions, respectively:

$$0 = -\rho_s \dot{R}\omega_s + \gamma_0(u_n - \dot{x}) + \dot{R}\gamma_0', \tag{C.4}$$

$$0 = \rho_s\omega_s(\dot{x} - u_s) - \gamma_0\dot{R} + \gamma_0'(u_n - \dot{x}). \tag{C.5}$$

The solution is obtained in the form:

$$\dot{x}(t) = \frac{\gamma_0^2\rho_s\omega_s(u_n - u_s)}{(\gamma_0^2 + (\gamma_0' - \rho_s\omega_s)^2)(\rho_s\omega_s - \gamma_0')} + \frac{u_s\rho_s\omega_s - \gamma_0' u_n}{\rho_s\omega_s - \gamma_0'}, \tag{C.6}$$

$$\dot{R}(t) = \frac{\gamma_0\rho_s\omega_s}{\gamma_0^2 + (\gamma_0' - \rho_s\omega_s)^2}(u_n - u_s). \tag{C.7}$$

To follow the position $x(t)$ and radius $R(t)$ of the dipole in time, we calculate:

$$x(t) = \int_0^t \dot{x}(s)ds, \quad R(t) = \int_0^t \dot{R}(s)ds. \tag{C.8}$$

References

[1] L. Tisza, Transport phenomena in Helium II, Nature 141 (1938) 913.
[2] L. Landau, Theory of the superfluidity of Helium II, Phys. Rev. 60 (1941) 356–358.
[3] C. Nore, M. Abid, M.E. Brachet, Decaying Kolmogorov turbulence in a model of superflow, Phys. Fluids 9 (1997) 2644–2669.
[4] C. Nore, M. Abid, M. Brachet, Kolmogorov turbulence in low-temperature superflows, Phys. Rev. Lett. 78 (1997) 3896–3899.
[5] P. Clark di Leoni, P.D. Mininni, M.E. Brachet, Dual cascade and dissipation mechanisms in helical quantum turbulence, Phys. Rev. A 95 (2017) 053636.
[6] M. Kobayashi, P. Parnaudeau, F. Luddens, C. Lothodé, L. Danaila, M. Brachet, I. Danaila, Quantum turbulence simulations using the Gross-Pitaevskii equation: high-performance computing and new numerical benchmarks, Comput. Phys. Commun. 258 (2021) 107579.
[7] N.G. Berloff, M. Brachet, N.P. Proukakis, Modeling quantum fluid dynamics at nonzero temperatures, Proc. Natl. Acad. Sci. 111 (2014) 4675–4682.
[8] I. Bekarevich, I. Khalatnikov, Phenomenological derivation of the equations of vortex motion in Helium II, Sov. Phys. JETP 13 (1961) 643.
[9] H.E. Hall, W.F. Vinen, D. Shoenberg, The rotation of liquid Helium II. I. Experiments on the propagation of second sound in uniformly rotating Helium II, Proc. R. Soc. Lond. Ser. A, Math. Phys. Sci. 238 (1956) 204–214.
[10] H.E. Hall, W.F. Vinen, D. Shoenberg, The rotation of liquid Helium II. II. The theory of mutual friction in uniformly rotating Helium II, Proc. R. Soc. Lond. Ser. A, Math. Phys. Sci. 238 (1956) 215–234.
[11] M.D. Bustamante, S. Nazarenko, Derivation of the Biot-Savart equation from the nonlinear Schrödinger equation, Phys. Rev. E 92 (2015) 053019.
[12] H. Adachi, S. Fujiyama, M. Tsubota, Steady-state counterflow quantum turbulence: simulation of vortex filaments using the full Biot-Savart law, Phys. Rev. B 81 (2010) 104511.
[13] D. Kivotides, C.F. Barenghi, D.C. Samuels, Triple vortex ring structure in superfluid helium II, Science 290 (2000) 777–779.
[14] L. Galantucci, A.W. Baggaley, C.F. Barenghi, G. Krstulovic, A new self-consistent approach of quantum turbulence in superfluid helium, Eur. Phys. J. Plus 135 (2020) 547.
[15] A.W. Baggaley, The sensitivity of the vortex filament method to different reconnection models, J. Low Temp. Phys. 168 (2012) 18–30.
[16] L. Galantucci, A.W. Baggaley, N.G. Parker, C.F. Barenghi, Crossover from interaction to driven regimes in quantum vortex reconnections, Proc. Natl. Acad. Sci. 116 (2019) 12204–12211.
[17] L. Galantucci, G. Krstulovic, C.F. Barenghi, Friction-enhanced lifetime of bundled quantum vortices, Phys. Rev. Fluids 8 (2023) 014702.
[18] G.W. Stagg, N.G. Parker, C.F. Barenghi, Superfluid boundary layer, Phys. Rev. Lett. 118 (2017) 135301.
[19] J. Koplik, H. Levine, Vortex reconnection in superfluid helium, Phys. Rev. Lett. 71 (1993) 1375–1378.
[20] T. Frisch, Y. Pomeau, S. Rica, Transition to dissipation in a model of superflow, Phys. Rev. Lett. 69 (1992) 1644.
[21] S. Balibar, Laszlo Tisza and the two-fluid model of superfluidity, in: Science in the Making: The Comptes Rendus de L'Académie des Sciences Throughout History, C. R. Phys. 18 (2017) 586–591.
[22] C. Coste, Nonlinear Schrödinger equation and superfluid hydrodynamics, Eur. Phys. J. B, Condens. Matter Complex Syst. 1 (1998) 245–253.
[23] E.B. Sonin, Magnus force in superfluids and superconductors, Phys. Rev. B 55 (1997) 485–501.
[24] E. Sandier, S. Serfaty, Vortices in the Magnetic Ginzburg-Landau Model, Birkhäuser, Boston, 2007.
[25] W. Bao, Y. Cai, Mathematical theory and numerical methods for Bose-Einstein condensation, Kinet. Relat. Models 6 (2013) 1–135.
[26] M. Tsubota, K. Fujimoto, S. Yui, Numerical studies of quantum turbulence, J. Low Temp. Phys. 188 (2017) 119–189.
[27] P. Parnaudeau, A. Suzuki, J.-M. Sac-Epée, GPS: an efficient & spectrally accurate code for computing Gross-Pitaevskii equation, in: ISC-2015, Research Posters Session, 2015.
[28] D. Gottlieb, S.A. Orszag, Numerical Analysis of Spectral Methods, SIAM, Philadelphia, 1977.
[29] M. Frigo, S. Johnson, Design and implementation of FFTW3, Proc. IEEE 93 (2005) 216–231.
[30] C. Nore, M.E. Brachet, E. Cerda, E. Tirapegui, Scattering of first sound by superfluid vortices, Phys. Rev. Lett. 72 (1994) 2593–2595.
[31] A. Griffin, V. Shukla, M.-E. Brachet, S. Nazarenko, Magnus-force model for active particles trapped on superfluid vortices, Phys. Rev. A 101 (2020) 053601.
[32] T.P. Billam, M.T. Reeves, B.P. Anderson, A.S. Bradley, Onsager-Kraichnan condensation in decaying two-dimensional quantum turbulence, Phys. Rev. Lett. 112 (2014) 145301.
[33] S. Inui, M. Tsubota, Coupled dynamics of quantized vortices and normal fluid in superfluid ^{4}He based on the lattice Boltzmann method, Phys. Rev. B 104 (2021) 214503.
[34] C.F. Barenghi, R.J. Donnelly, W.F. Vinen, Friction on quantized vortices in Helium II. A review, J. Low Temp. Phys. 52 (1983) 189–247.
[35] M.V. Melander, F. Hussain, Cross-linking of two antiparallel vortex tubes, Phys. Fluids A, Fluid Dyn. 1 (1989) 633–636.
[36] F. Hussain, K. Duraisamy, Mechanics of viscous vortex reconnection, Phys. Fluids 23 (2011) 021701.
[37] N.G. Berloff, P.H. Roberts, Motions in a Bose condensate: VI. Vortices in a nonlocal model, J. Phys. A, Math. Gen. 32 (1999) 5611–5625.
[38] N.P. Müller, G. Krstulovic, Critical velocity for vortex nucleation and roton emission in a generalized model for superfluids, Phys. Rev. B 105 (2022) 014515.
[39] N.P. Müller, G. Krstulovic, Kolmogorov and Kelvin wave cascades in a generalized model for quantum turbulence, Phys. Rev. B 102 (2020) 134513.